Density Functional Theory and Molecular Dynamics Simulation of Poly(dimethylsiloxane) Melts near Silica Surfaces

Shyamal K. Nath,*,† Amalie L. Frischknecht,‡ John G. Curro,‡,§ and John D. McCoy†

Department of Materials Engineering, New Mexico Tech, Socorro, New Mexico 87801; Sandia National Laboratories, Albuquerque, New Mexico 87185; and Department of Chemical & Nuclear Engineering, University of New Mexico, Albuquerque, New Mexico 87131

Received May 13, 2005; Revised Manuscript Received July 22, 2005

ABSTRACT: Classical density functional theory (DFT) is applied to study properties of fully detailed, realistic models of poly(dimethylsiloxane) liquids near silica surfaces and compared to results from molecular dynamics simulations. In solving the DFT equations, the direct correlation functions are obtained from the polymer reference interaction site model (PRISM) theory for the repulsive parts of the interatomic interactions, and the attractions are treated via the random-phase approximation (RPA). Good agreement between density profiles calculated from DFT and from the simulations is obtained with empirical scaling of the direct correlation functions. Separate scaling factors are required for the PRISM and RPA parts of the direct correlation functions. Theoretical predictions of stress profiles, normal pressure, and surface tensions are also in reasonable agreement with simulation results.

I. Introduction

Poly(dimethylsiloxane) (PDMS) is a very important polymer for its application in the adhesives, sealants, coatings, and biomedical industries. PDMS is the simplest of the silicones, possesses a hydrophobic surface, and is highly surface active. Because of such properties, it is used as an aqueous foam-control agent in the coatings industry. In the adhesives and sealants industry, PDMS is often used to graft silica surfaces with inert functional groups to modify properties. In the adhesives industry, fumed silica is used to increase the product viscosity, improve antisettling properties during storage, control the extrusion properties during application, and impart antisag properties during cure. Fumed silica also acts as a reinforcing agent to improve the physical properties of cured sealants. In the biomedical applications, layers of silica and PDMS are used around magnetic cobalt nanoparticles to inhibit environmental oxidation.[1]

Despite such important applications, our understanding of the properties of PDMS near silica is limited. Not many experimental, theoretical, or simulation studies have been devoted to the understanding of molecular level structure and thermodynamics of such systems. Horn and Israelachvili[2] studied the force between two molecularly smooth mica surfaces immersed in liquid PDMS using the surface force apparatus.[3] Tsige et al.[4] studied the properties of thin PDMS films on hydroxylated SiO_2 substrates, using fully atomistic molecular dynamics simulations and ab initio methods. The main purpose of this work is to study properties of a fully detailed, realistic model of PDMS near silica surfaces using classical density functional theory. In contrast to well-known *electronic density functional theory* used in ref 4, in this paper we refer to *classical density functional theory* with the shorthand DFT. DFT is an attractive method for obtaining the properties of polymers near surfaces, in that it is much less computationally expensive than simulations and yields equilibrium properties directly. However, the application of DFT to atomistically detailed models is quite new. Thus, here we also conduct full-scale molecular dynamics (MD) simulations of the same system to compare to our theoretical work.

Our molecular density functional theory is based on the class of theories that uses the structure of the homogeneous liquid as input. Structure-based density functional theory was first extended to molecular systems by Chandler, McCoy, and Singer (CMS).[5−7] Sen et al.[8,9] first used this theory in studying properties of polymers near surfaces. They studied a homopolymer tridecane melt near a hard surface. In their study, the intrachain interactions of tridecane molecules were formulated within the rotational-isomeric-state[10] (RIS) model, and the interchain interactions were hard in nature. They showed that almost quantitative agreement with molecular dynamics simulation of a Lennard-Jones tridecane could be obtained by adjusting the hard-sphere diameter of the methylene group in their model tridecane molecules. To the best of our knowledge, this was the most detailed polymer model that has been studied within the CMS density functional theory until recently.

In recent work,[11] we have used the CMS density functional theory to study fully detailed, realistic models (within the united atom framework) of polyethylene molecules near attractive surfaces. Like other structure-based DFT applications, direct correlation functions, in that work, were obtained from the polymer reference interaction site model[12] (PRISM) theory with attractions treated via the random-phase approximation[13] (RPA). We demonstrated that, with empirical scaling of the PRISM-RPA predicted direct correlation functions, almost quantitative results could be obtained from density functional treatment of atomistically detailed realistic polymer models. Other formulations of DFT that use the equation of state of the bulk liquid as input have also been developed and applied to polymers.[14−17]

† New Mexico Tech.
‡ Sandia National Laboratories.
§ University of New Mexico.
* To whom correspondence should be addressed. E-mail: shyam_nath@hotmail.com.

10.1021/ma051001k CCC: $30.25
Published on Web 08/30/2005

From a theoretical perspective, this work is a step forward from our previous study[11] in that here we apply density functional theory to a more complex molecular system. PDMS has a more complex architecture compared to polyethylene. Within the united atom framework, PDMS consists of three different types of interaction sites: silicon (Si), methyl (CH_3), and oxygen (O). In our previous work, polyethylene was modeled as a linear chain of a single type of interaction site, namely methylene.

In this work we use the CMS density functional theory to study properties of full, atomistically detailed (within the united atom framework) PDMS chains of various length near silica surfaces. We also conducted full-scale molecular dynamics simulations of the same systems and compared to our theoretical predictions. To increase the efficiency of the density functional theory computations, following previous work, we decouple the single chain simulation step from the iterative solution by the use of an umbrella potential and use of reweighting techniques.[11,18]

We describe the model PDMS system in section II. We then briefly review the CMS-DFT as applied here to a thin film of PDMS in section III, along with the calculation of mechanical properties from the DFT. The details of our MD simulations are given in section IV. Results and comparisons between the two methods are presented in section V.

II. Model

We model our PDMS chains within the united atom framework, where the Si and O atoms are treated explicitly while each methyl group (CH_3) is treated as a single particle. We use the force field parameters developed by Frischknecht and Curro,[19] which have been optimized to provide the correct structure of bulk PDMS at liquid densities. This force field was also successfully used in a recent study of cross-linked PDMS networks.[20] This force field, hereafter referred to as the hybrid/UA model, is a class I type force field. Thus, the bond lengths vary around a preferred length r_0 in a harmonic potential

$$V_b(r) = K_b(r - r_0)^2 \tag{1}$$

as do the bond angles about a fixed angle θ_0:

$$V_a(\theta) = K_\theta(\theta - \theta_0)^2 \tag{2}$$

The torsional angles, φ, are subject to a torsional potential of the form

$$V_t(\varphi) = K_t(1 + \cos n\varphi) \tag{3}$$

The nonbonded interactions, and interactions between atoms separated by more than three bonds in the same molecule, are represented using two different forms of the Lennard-Jones (LJ) potential. A 9−6 LJ model is used for the Si, O, and Si−O interactions

$$V_{\alpha\gamma}(r) = \epsilon_{\alpha\gamma}\left[2\left(\frac{\sigma_{\alpha\gamma}}{r}\right)^9 - 3\left(\frac{\sigma_{\alpha\gamma}}{r}\right)^6\right], \quad \alpha \text{ and } \gamma = \{\text{Si, O}\} \tag{4}$$

and a 12−6 LJ model is used for the interactions involving the methyl groups:

$$V_{\alpha\gamma}(r) = 4\epsilon_{\alpha\gamma}\left[\left(\frac{\sigma_{\alpha\gamma}}{r}\right)^{12} - \left(\frac{\sigma_{\alpha\gamma}}{r}\right)^6\right], \quad \alpha \text{ or } \gamma = CH_3 \tag{5}$$

Parameters associated with the bonded and nonbonded interactions are given in Table 1.[21]

The original hybrid/UA model[19] contains partial charges on the Si and the O atoms. However, one of the important findings of that work was that partial charges in PDMS have very little effect on the molecular structure of its bulk liquid. Thus, we ignore the partial charges in PDMS throughout this work.

As will be described below, the PRISM theory needed as input to the DFT is solved with the repulsive part of the LJ interactions. To this end, we decompose the full 12−6 LJ interaction into a repulsive part $V^{rep}(r)$

$$V^{rep}(r) = 4\epsilon\left[\left(\frac{\sigma}{r}\right)^{12} - \left(\frac{\sigma}{r}\right)^6\right] + \epsilon, \quad r \le 2^{1/6}\sigma$$
$$= 0, \quad r > 2^{1/6}\sigma \tag{6a}$$

and an attractive or perturbative part $V^{att}(r)$

$$V^{att}(r) = -\epsilon, \quad r \le 2^{1/6}\sigma$$
$$= 4\epsilon\left[\left(\frac{\sigma}{r}\right)^{12} - \left(\frac{\sigma}{r}\right)^6\right], \quad r > 2^{1/6}\sigma \tag{6b}$$

For the 9−6 LJ interactions, we decompose the potential as

$$V^{rep}(r) = \epsilon\left[2\left(\frac{\sigma}{r}\right)^9 - 3\left(\frac{\sigma}{r}\right)^6\right] + \epsilon, \quad r \le \sigma$$
$$= 0, \quad r > \sigma \tag{7a}$$

and

$$V^{att}(r) = -\epsilon, \quad r \le \sigma$$
$$= \epsilon\left[2\left(\frac{\sigma}{r}\right)^9 - 3\left(\frac{\sigma}{r}\right)^6\right], \quad r > \sigma \tag{7b}$$

While working with attractive systems, we also truncate the attractive tail at a distance of 12 Å and shift the whole curve such that the potential is zero at the cutoff.

Our system consists of a PDMS liquid confined in a slit between two silica surfaces. The two surfaces are placed a distance D apart from each other in the z direction, and the system is considered infinite in both the x and the y directions. Both the walls are identical and interact uniformly with the polymer fluid.

Two different surface potentials are considered here, both of which are representative of a wall containing oxygen atoms to represent an amorphous silica surface. The first is obtained by integrating the LJ potential for the interaction between an atom of type i and the surface over all points in the infinite half-plane representing the wall and retaining only the repulsive contribution, giving a repulsive wall potential:

$$V_i(z) = 2\pi\rho_w\epsilon_{wi}\begin{cases}\left(\frac{\sigma_{wi}}{21z}^9\right) & i = \text{Si, O} \\ \left(\frac{2\sigma_{wi}}{45z^9}^{12}\right) & i = CH_3\end{cases} \tag{8}$$

We take the density of atoms in the wall to be $\rho_w\sigma_w^3 =$

Table 1. Force Field Parameters of Frischknecht and Curro[19,21] for PDMS

bonds	r_0 [Å]	K_b [kcal/(mol Å^2)]
Si−O	1.64	350.12
Si−CH_3	1.90	189.65
angles	θ_0 [deg]	K_θ [kcal/(mol rad^2)]
Si−O−Si	146.46	14.14
O−Si−O	107.82	94.5
CH_3−Si−CH_3	109.24	49.97
O−Si−CH_3	110.69	49.97
dihedrals	n	K_t [kcal/mol]
Si−O−Si−O	1	0.225
Si−O−Si−CH_3	3	0.01
nonbonded	σ [Å]	ϵ [kcal/mol]
Si−Si	4.29	0.1310
Si−O	3.94	0.0772
Si−CH_3	3.83	0.1596
O−O	3.30	0.0800
O−CH_3	3.38	0.1247
CH_3−CH_3	3.73	0.1944

1.0, where the wall consists of oxygen atoms with $\sigma_w = \sigma_O = 3.3$ Å. The wall−atom interactions were chosen to be the same as in the PDMS model for oxygen−atom interactions, $\sigma_{wi} = \sigma_{oi}$ and $\epsilon_{wi} = \epsilon_{oi}$.

The second potential comes from integrating only over the surface plane that is assumed to consist of some density of oxygen atoms, representing the −OH groups on the surface, resulting in

$$V_i(z) = 2\pi\rho_{ws}\epsilon_{wi}\begin{cases}\left(\dfrac{2\sigma_{wi}^{9}}{7z^{7}} - \dfrac{3\sigma_{wi}^{6}}{4z^{4}}\right) & i = \text{Si, O}\\ \left(\dfrac{2\sigma_{wi}^{12}}{5z^{10}} - \dfrac{\sigma_{wi}^{6}}{z^{4}}\right) & i = \text{CH}_3\end{cases} \quad (9)$$

Here the surface density of OH groups was taken to be that found in an atomistic simulation of amorphous silica,[4] $\rho_{ws} = 0.039$ Å^{-2}. The wall−atom interactions were chosen as before, $\sigma_{wi} = \sigma_{oi}$ and $\epsilon_{wi} = \epsilon_{oi}$.

We considered three different sizes of PDMS molecules in the DFT study, namely, PDMS24 (6-mer PDMS with a total of 24 interaction sites), PDMS48 (12-mer PDMS), and PDMS80 (20-mer PDMS). For full-scale MD simulations, due to the high demand of computational resources, only PDMS80 system was considered. All the calculations were performed at 298.0 K (except the MD simulations which were at 300 K; the difference is negligible) and at the experimental density of PDMS of 0.98 g/cm^3. The separation between the two surfaces was set to 60 Å throughout this study, unless otherwise mentioned.

III. Density Functional Theory

A. Theory. The essence of the density functional theory formalism is to map the real system of interest onto an ideal system of noninteracting chains immersed in a medium-induced (mean) field. For a known medium-induced field, the density profile of the real system can then be estimated from simulations of a single chain in the presence of the field. A detailed derivation of the general density functional methodology has already appeared in the literature.[18,22] Here, we merely summarize the system of equations that must be solved in our context.

Consider a polymer melt composed of chains with N spherical interaction sites, in volume V, at temperature T, and chemical potential μ. The system has an inhomogeneous monomer density profile $\rho(\mathbf{r}) = \sum_\alpha \rho_\alpha(\mathbf{r})$, where $\rho_\alpha(\mathbf{r})$ is the density of site type α at $\mathbf{r}$. In the density functional theory formalism, the free energy of the system is constructed in a somewhat nonconventional grand canonical ensemble with T, V, $\rho(\mathbf{r})$, and ψ as independent variables. Here, $\psi = \mu - U_\alpha(\mathbf{r})$; $U_\alpha(\mathbf{r})$ represents an external field, such as that due to surfaces, acting on each site of type α. Note that, in a conventional grand canonical ensemble, $\rho(\mathbf{r})$ is not an independent variable. In the CMS-DFT, an excess Helmholtz free energy is defined relative to an ideal reference system, and the excess free energy of the system is constructed as a Taylor series expansion about the homogeneous liquid state, truncated after the second order. The grand potential is then related to the excess free energy with a Legendre transform. A functional minimization of the grand potential free energy with respect to the density fields provides the required expression for the medium-induced field, which, along with the definition of the ideal system, constitutes the set of density functional equations.

The ideal system we use is a collection of noninteracting chains in the medium-induced field and experiencing the same intramolecular interactions as the real system. The ideal system can be defined according to

$$\rho_\beta(\mathbf{r}) = \int\!\!\ldots\!\int \exp[\sum_\alpha \psi_\alpha^{\text{id}}(\mathbf{r}_\alpha)] S(\mathbf{r}_1,\ldots,\mathbf{r}_N) \prod_{\alpha\neq\beta} \mathrm{d}\mathbf{r}_\alpha \quad (10)$$

where $\rho_\beta(\mathbf{r})$ is the density of the β-th site in the polymer chain, the sums and products are over the N sites of the chain, and S is the N-body correlation function for a molecule of N sites. The function S restores the exact intramolecular interactions between all sites of an individual chain in the real system. $\psi_\alpha^{\text{id}}(\mathbf{r}_\alpha) = \mu^{\text{id}} - U_\alpha^{\text{m}}(\mathbf{r}_\alpha)$, where $U_\alpha^{\text{m}}(\mathbf{r}_\alpha)$ is the medium-induced field (plus the wall potential in our case) on the α-th site of the ideal chain molecule.

Derivation of the density functional equation with the above ideal system leads to the following expression for the medium-induced field

$$\beta U_\alpha^{\text{m}}(\mathbf{r}) = \beta U_\alpha(\mathbf{r}) - \sum_\beta \int_V \mathrm{d}\mathbf{r}'\, c_{\alpha\beta}(|\mathbf{r}-\mathbf{r}'|)\rho_\beta(\mathbf{r}') + \text{constant} \quad (11)$$

where $\beta = 1/k_B T$, with k_B being the Boltzmann constant, $U_\alpha(\mathbf{r})$ is the external field due to the presence of the surface, and $c_{\alpha\beta}(\mathbf{r}-\mathbf{r}')$ is the direct correlation function between the α-th and the β-th site in the bulk polymer fluid. The constant in eq 11 is related to the chemical potential but does not need to be evaluated for the calculations here. For systems where the distance between the walls are sufficient enough to ensure bulk behavior in the middle, we effectively set the constant to zero and obtain the required normalization of the density profiles by setting the appropriate density at the midpoint of the simulation box. The excess grand potential free energy of the inhomogeneous system (relative to the bulk homogeneous system) is

$$\Delta\Omega = -\frac{1}{N}\sum_{\alpha}\int d\mathbf{r}\,(\rho_{\alpha}(\mathbf{r}) - \rho_{\alpha,b}) + \frac{1}{2}\sum_{\alpha\beta}\int\int d\mathbf{r}\,d\mathbf{r}'\,c_{\alpha\beta}(|\mathbf{r}-\mathbf{r}'|)[\rho_{\alpha}(\mathbf{r})\rho_{\beta}(\mathbf{r}') - \rho_{\alpha,b}\rho_{\beta,b}] \quad (12)$$

The density profile for the inhomogeneous system is obtained by performing a single chain (ideal system) simulation in the medium-induced (ideal) field. In this work we perform a Monte Carlo simulation of the single chain as described below. Since both the density and the field are coupled through eq 11, a self-consistent solution is required. We use a simple Picard iteration scheme to obtain such a solution.

To increase the computational efficiency of the density functional equations, Hooper et al.[18] proposed a decoupling of the simulation step by using an umbrella potential. The single chain simulation is performed under an additional external umbrella field prior to starting the self-consistent simulation loop, and chain configurations at a certain interval are saved. The density distribution, for any given medium-induced field, is then obtained from the weighted average:

$$\rho_{\alpha}(\mathbf{r}) = \langle\delta(|\mathbf{r}-\mathbf{r}_{\alpha}|)\exp(-\beta\sum_{\beta=1}^{N}[U_{\alpha}^{m}(\mathbf{r}_{\beta}) - U_{U}(\mathbf{r}_{\beta})])\rangle \quad (13)$$

where $U_U(\mathbf{r}_\beta)$ is the umbrella potential for the β-th site. Following Hooper et al.,[18] we use a starting umbrella potential of the form

$$\beta U_{U}(z) = a\left(\frac{z - z_{center}}{z_{center}}\right)^4 \quad (14)$$

where a is an arbitrary constant and z_{center} is halfway between the walls. We used an a value of -0.1 to -0.3 for methyl and oxygen sites and an a value of 0.1 to 0.3 for silicon sites (the hidden sites in PDMS). Without an umbrella potential the single polymer chain would be distributed more or less randomly between the surfaces. The umbrella potential in eq 14 forces the chain to spend more time near the surfaces and thus improves the sampling required to obtain density profiles near the surfaces. The use of umbrella potentials is discussed in ref 23.

To ensure the accuracy of the obtained DFT solutions using the umbrella-sampling scheme, we perform a two-loop solution following our previous work.[11] First, we choose an arbitrary (e.g., eq 14) umbrella potential and obtain the iterative density functional theory solution. After self-consistency is achieved between the density profile and the medium-induced potential from using the configurations from the umbrella potential, we perform another simulation using the final potential to verify our results. If there are discrepancies between the density profiles, we restart the self-consistency loop with the new set of configurations and the self-consistent potential from the last loop as our new umbrella potential.

B. Mechanical Properties. Once we have a solution to the DFT, we can calculate some additional properties beyond just the density profile. In our formulation of the DFT, the excess surface free energy Ω^{ex}/A is the free energy difference per unit area between the wall–polymer system of interest and the bulk polymer at the same density (far from the wall). This excess surface free energy can be identified as the surface or interfacial tension, γ:[24]

$$\gamma = \Omega^{ex}/A \quad (15)$$

and is obtained directly from eq 12. The surface tension can also be calculated from the components of the pressure tensor. In planar symmetry such as we have here, the off-diagonal components of the pressure tensor vanish and the lateral components are identical. Furthermore, the pressure can only be a function of the distance z from the surface, so we find that the normal component $P_N(z) = P_{zz} = \text{constant} = p$ (the bulk pressure far from the surface) and the lateral component $P_T(z) = P_{xx}(z) = P_{yy}(z)$. The mechanical definition of the surface tension is

$$\gamma = \int_{-\infty}^{\infty} dz\, s(z) = \int_{-\infty}^{\infty} dz\,[P_N - P_T(z)] \quad (16)$$

where $s(z)$ is the stress profile across the interface.[25,26]

Thermodynamically, the grand free energy density can be identified with the lateral pressure $P_T(z)$.[25] Thus, on the basis of eqs 15 and 16, we can identify the stress profile across the interface with the excess free energy density, i.e., $s(z) = \Omega^{ex}(z)/A$, so that we have

$$s(z) = -\frac{1}{N}\sum_{\alpha}[\rho_{\alpha}(z) - \rho_{\alpha,b}] + \frac{1}{2}\sum_{\alpha\beta}\int d\mathbf{r}'\,c_{\alpha\beta}(|\mathbf{r}-\mathbf{r}'|)[\rho_{\alpha}(z)\rho_{\beta}(z') - \rho_{\alpha,b}\rho_{\beta,b}] + S \quad (17)$$

Here S is a constant arising from bulk polymer and can be most easily evaluated by setting $s(z) = 0$ in the bulk system far from the surface. This expression was recently used by Frischknecht and Frink to calculate the stress profile across a lipid bilayer using the CMS-DFT.[27] In this work, $s(z)$ is an additional quantity beyond the density profiles $\rho(z)$ that we can compare to simulation.

The normal component of the pressure tensor, P_N, can also be directly calculated from the density profiles of the polymers near the surface using the wall sum rule. As has been demonstrated by Rickayzen,[28] the wall sum rule for the partial pressure on the wall due to interaction site type α and for wall–polymer interaction potential $v_\alpha(z)$ is

$$\beta P_{\alpha} = \rho_{\alpha w} - \beta\int_0^{\infty} dz\,\frac{\partial v_{\alpha}(z)}{\partial z}\,\rho_{\alpha}(z) \quad (18)$$

where $\rho_{\alpha w}$ is the wall contact density (which is zero for the type of wall–polymer interactions used in the work) and z is the distance from a single wall. The total normal pressure for any given wall–wall separation D is then

$$P_N(D) = \sum_{\alpha} P_{\alpha} \quad (19)$$

C. Direct Correlation Functions. The direct correlation functions of the bulk polymer system are required as input to the density functional theory in eq 11 for the mean field. The direct correlation functions are obtained using the polymer reference interaction site model[12] (PRISM) theory with the atomic Percus–Yevick (PY) closure. PRISM theory is an extension to polymers

of the reference interaction site model or RISM theory of Chandler and Andersen[29] for small molecule liquids. The atomic PY relation is most successful in describing the packing structure in simple hard-core liquids. However, it does not work well when attractive tail interactions are present. We make use of the fact that for dense polymer liquids the structure is primarily determined by the repulsive part of the potential. Consequently, for our model PDMS molecules where intermolecular interactions are of the LJ form, we use PRISM to obtain the correlations for the repulsive part of the interactions and use a perturbation scheme following the random-phase approximation[13] (RPA) to treat the attractive tail. Molecular closures[12] and other closures[30] that include attractions have also been used with PRISM theory but are beyond the scope of the present study.

With the RPA approximation, the direct correlation function between site types α and β is

$$c_{\alpha\beta}(r) = c_{\alpha\beta}^{\mathrm{rep}}(r) - \beta V_{\alpha\beta}^{\mathrm{att}}(r) \tag{20}$$

where $c^{\mathrm{rep}}(r)$ is the direct correlation function for repulsive interactions calculated from PRISM and $V^{\mathrm{att}}(r)$ is the attractive part of the nonbonded potential. We have used the same scheme to obtain the direct correlation functions in our DFT study of fully detailed polyethylene chains near realistic surfaces, with good success.[11] We also use the self-consistent version of PRISM theory, in which the intramolecular structure is obtained by simulating the isolated chain in the presence of a solvation potential that depends on the intermolecular packing of the liquid.[12]

Unfortunately, PRISM is known to overestimate the compressibility of the liquids. Curro et al.[31] conducted a self-consistent PRISM study of polyethylene-like molecules with a soft repulsive potential and found that the compressibility obtained from the theory is about 2−3 times higher than that obtained from MD simulations. In terms of the direct correlation function, the range of the function obtained from PRISM is exactly the same as the range of the intermolecular potential due to the inherent approximation built into the PY relation, whereas the direct correlation functions predicted from MD simulations were longer ranged compared to those obtained from the theory.

Sides et al.[32] previously conducted a self-consistent PRISM study of the united atom PDMS model of Sok and Berendsen.[33] Although the Sok−Berendsen model of PDMS is not optimized to provide the correct structure of the bulk liquid, the PRISM-predicted structure for PDMS in that study is a good representation of the quality of results that should be expected from PRISM for PDMS. Their study showed that PRISM-predicted pair correlation functions are only in qualitative agreement with MD simulations of the same system. Moreover, because of numerical errors, some of the PRISM-predicted pair correlation functions also showed spurious negative values. No direct comparison between the PRISM-predicted direct correlation functions and MD simulations for repulsive PDMS models were shown in that work. However, on the basis of the knowledge that PRISM theory is less accurate for systems with overlapping sites and the results of Sides et al.,[32] one would expect that PRISM-predicted direct correlation functions would be less accurate for PDMS than are those for polyethylene.

As seen in earlier work on polyethylene[11] and bead−spring[34] polymers, the DFT/PRISM approach gives good qualitative and sometimes quantitative agreement with simulation. To make the theory more useful for quantitative predictions, it is necessary to compensate for the combined effects of approximations in the bulk direct correlation functions from PRISM theory and the approximate form of the mean field in eq 11. Toward this end we follow the approach used by Frischknecht and Curro[34] and in our previous study[11] and include an adjustable multiplicative factor in the PRISM direct correlation functions used as input to DFT.

$$c_{\alpha\beta}(r) = K_1 c_{\alpha\beta}^{\mathrm{PRISM}}(r) \tag{21}$$

The bulk compressibility is proportional to $c(r)$, and thus the added factor essentially allows us to correct the compressibility. For attractive systems, we include an additional parameter to adjust the strength of the attractions:

$$c_{\alpha\beta}(r) = K_1 c_{\alpha\beta}^{\mathrm{rep,PRISM}}(r) - K_2 \beta V_{\alpha\beta}^{\mathrm{att}}(r) \tag{22}$$

The same two adjustable constants K_1 and K_2 are applied to all six of the direct correlation functions of PDMS needed as input to DFT theory. These constants can be determined by comparison with computer simulations (if available) or from the experimental equation of state. It should be emphasized that similar phenomenological modifications are required in the weighted-density DFT theory of atomic liquids[35] and polymer liquids[15] where separate weighting functions are needed for the repulsive and attractive contributions to the excess free energy. In fact in weighted DFT the equation of state of the bulk uniform liquid is used as input.

D. Monte Carlo Simulations. Two types of Monte Carlo simulations were carried out in obtaining the DFT solutions. The first is the simulation of a single chain in the solvation potential provided by the self-consistent PRISM theory. The second is the simulation of a single chain in the presence of the medium-induced and/or umbrella potentials during the DFT solution. In all the Monte Carlo simulations, we used three different types of moves: pivot bending, pivot torsion, and translation. Complete details of the Monte Carlo moves and the single chain Monte Carlo simulations performed during PRISM and DFT calculations are given in our previous publication.[11]

In obtaining the density profiles from the single chain simulation during the DFT solution, symmetry conditions were used to average the density profiles around the symmetry line between the two walls. The density at the midpoint between the two walls is set to the bulk density, since for large enough separation between the two walls the midpoint is unaffected by the surface. When solving the density functional equations using a Picard iteration scheme, it is necessary to mix the "old" and "new" density profiles at every step of the iteration procedure. We mix 5% of the "new" density profile at every step of the iteration.

Although our main focus in the present study is the overall density profile of the PDMS chains near a silica surface, the distribution of chain ends near the surface could also be extracted from the Monte Carlo simulation. In addition, detailed information regarding the PDMS structure near the surface (e.g., the existence of loops

and tails) could be obtained but is beyond the scope of the present investigation.

IV. Molecular Dynamics Simulations

As mentioned above, all the MD simulations were done on systems of 80 chains with 20 Si atoms per chain, at a density of 0.98 g/cm^3 and a temperature of $T = 300$ K in the NVT ensemble. An initial configuration of a methyl-terminated PDMS chain was prepared as described in ref 19. The configuration of this chain was then copied, rotated by a random angle about its center of mass, and the center-of-mass placed in a random position in the simulation box. To prepare a PDMS liquid between two confining surfaces, configurations in which the chain passed through the edges of the box in the z direction were discarded and the placement was tried again. Periodic boundary conditions were applied in the x and y directions, and the surface potentials of either eq 8 or eq 9 were used for the surfaces. Overlaps were removed using a soft nonbonded potential. The Lennard-Jones interactions were then turned on, using a time step of $\delta t = 0.4$ fs. In all simulations we used a multiple-time step integrator (RESPA) so that forces were calculated every time step for bonded interactions, every two time steps for three- and four-body forces, and every four time steps for van der Waals forces. The temperature T was controlled with a Nose-Hoover thermostat using a coupling frequency of 0.02 fs^{-1}.

We began with the repulsive wall potential of eq 8 and equilibrated the system at an elevated temperature of $T = 600$ K for 1.3 ns, after which the chains' center of mass had moved an average distance of 17.7 Å, about twice the radius of gyration of the chains (here $R_g = 8.76 \pm 0.03$ Å). The temperature was then lowered to 300 K and the system equilibrated further until the chains moved one more radius of gyration. A second simulation using the wall potential of eq 9 was started from the previously equilibrated system near the repulsive wall at 300 K. In both cases statistics to calculate density profiles were then collected for 2.4 ns, sampling configurations every 0.04 ns. The simulations were run on 16 processors on the Sandia CPlant cluster, using the parallel LAMMPS MD code.[36]

We can calculate the surface tension of the film from the components of the averaged stress tensor $\Sigma^{\alpha\beta}$ using the mechanical definition of the surface tension:

$$2\gamma = \int_{-D}^{D} \mathrm{d}z\, s(z) = \int_{-D}^{D} \mathrm{d}z\, [P_N(z) - P_T(z)] \quad (23)$$

where the factor of 2 accounts for the two surfaces, and

$$\Sigma^{\alpha\beta} = \begin{pmatrix} -P_T & 0 & 0 \\ 0 & -P_T & 0 \\ 0 & 0 & -P_N \end{pmatrix} \quad (24)$$

for the planar symmetry considered here. The macroscopic stress tensor $\Sigma^{\alpha\beta}$ can be calculated from the thermal average of the microscopic stress tensor $\sigma^{\alpha\beta}$, $\Sigma^{\alpha\beta} = \langle\sigma^{\alpha\beta}\rangle$. An early definition of $\sigma^{\alpha\beta}$ was given by Irving and Kirkwood[37] and is commonly used to calculate the surface tension in simulations. However, some time ago Schofield and Henderson showed that the microscopic stress tensor, as defined by the conservation of linear momentum density, is not unique.[38] This is essentially due to the fact that it is unclear exactly where the configurational part of the stress due to interactions between atoms acts. More recently, Wajnryb et al.[39] have argued that imposing some additional physically reasonable constraints leads to a unique definition for $\sigma^{\alpha\beta}$, which is in fact the original stress tensor defined by Irving and Kirkwood (IK). Additionally, one of the alternative definitions for $\sigma^{\alpha\beta}$ given by Harasima[40] has been shown to fail in spherical coordinates and is thus not a valid definition for $\sigma^{\alpha\beta}$.[41] Thus, in this work we calculate the components of $\sigma^{\alpha\beta}$ using the IK definition.[37] In any case, the value of the surface tension from eq 23 is independent of the choice of stress tensor and thus well-defined.[38]

Goetz and Lipowsky[42] extended the work of Schofield and Henderson to calculate the contribution of many-body forces to the IK stress tensor $\sigma^{\alpha\beta}$. We use their formulas for the contribution of the angle and dihedral forces in PDMS to $\sigma^{\alpha\beta}$. The contributions of the bond forces and nonbond Lennard-Jones forces are calculated using the usual IK stress. Finally, there is also a contribution from the surfaces to the normal pressure which can be computed by considering each wall as an additional particle of infinite mass as shown by Varnik et al.[43] To apply these formulas to the MD simulation, we bin the local stress in slabs parallel to the surfaces and employ the Hardy method.[44] Because of large fluctuations, the stress tensor components were calculated every 1000 time steps (every 0.4 ps) and averaged for a total of 2 ns. The transverse pressure was calculated as an average of the xx and yy components, $P_T = (P_{xx} + P_{yy})/2$. The normal pressure was found to be constant throughout the films, as required by mechanical stability.[25,43]

V. Results

A. Direct Correlation Functions. We begin the Results section by looking at the pair correlation and direct correlation functions of PDMS, obtained from PRISM calculations. Although PRISM predictions of bulk polymer correlations of PDMS and similar molecules have previously appeared in the literature,[32] we present our results here to refresh the readers with the nature of the direct correlation functions observed for PDMS. Also note that earlier PRISM work on PDMS used an interaction potential model that was not well optimized for structure of bulk liquid. Thus, our results also clarify if the observations of Sides et al.[32] hold true when a more accurate set of force field parameters are used.

Intermolecular pair correlation functions for all six pairs of site−site interactions, obtained using the PRISM-PY theory for bulk repulsive PDMS80 (eqs 6a and 7a), are shown in Figure 1. The Si−Si, Si−O, Si−CH_3, and O−O pair correlations all show some unrealistic negative values, with Si−Si and O−O having the most prominent effects. Sides et al. observed the same phenomena in their PRISM work with the Sok−Berendson united atom PDMS model. As expected, correlations involving Si sites have the most of the unrealistic features, and the correlations involving CH_3 sites have the least. The Si sites are the most overlapped in the PDMS structure, and PRISM is known to be less accurate for overlapping (hidden) sites.

Direct correlation functions for all six pairs of site−site interactions for the above system are shown in Figure 2. An interesting feature of the direct correlation functions is that the correlations have positive values within the repulsive core for interactions involving Si sites. In terms of the DFT equations (eq 11), this means

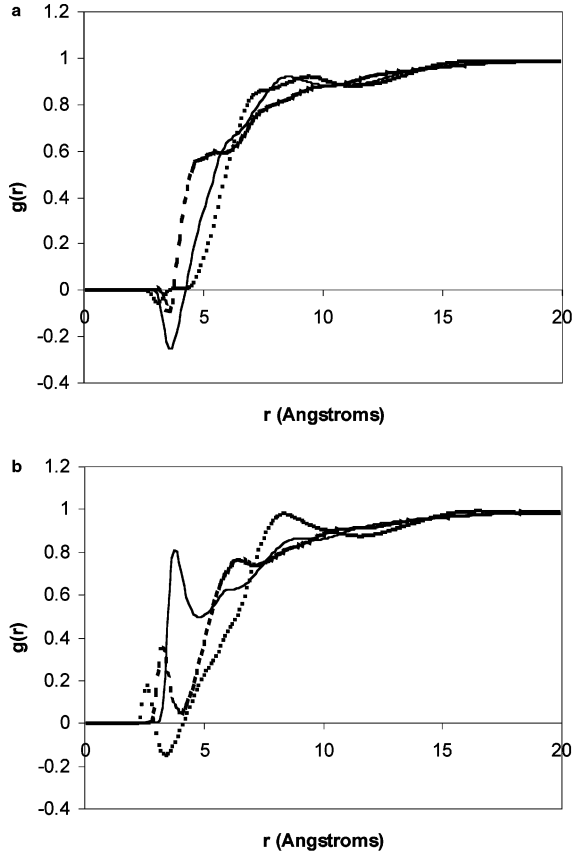

Figure 1. Pair correlation functions, $g(r)$, of 20-mer PDMS molecules at 298 K and 0.98 g/cm^3. (a) The dashed, dotted, and solid lines correspond to Si−CH_3, Si−O, Si−Si interactions, respectively. (b) The dashed, dotted, and solid lines correspond to CH_3−O, O−O, and CH_3−CH_3 interactions, respectively.

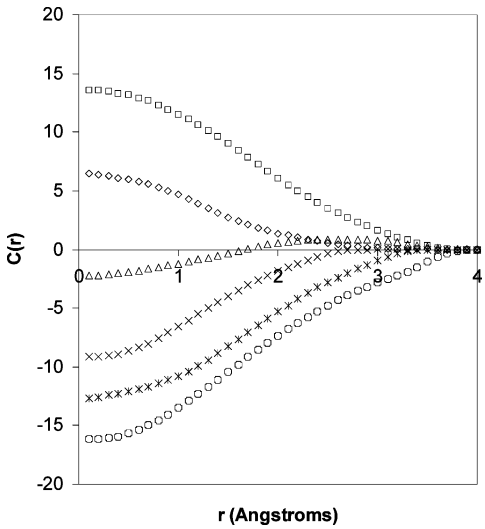

Figure 2. Direct correlation functions, $C(r)$, of 20-mer PDMS molecules at 298 K and 0.98 g/cm^3. The meanings of symbols are as follows: squares (Si−CH_3), diamonds (Si−O), triangles (Si−Si), crosses (O−O), asterisks (CH_3−O), and circles (CH_3−CH_3).

that with a given density profile of the system the medium-induced potential for Si would drive the density profile near the surface in the opposite direction to the potentials for O and CH_3 sites. This opposite trend in the medium-induced potentials makes the solution of the DFT equations for PDMS more delicate than that

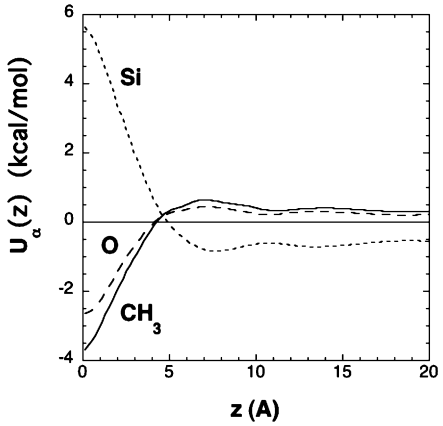

Figure 3. Typical medium-induced potentials for Si (short dash), CH_3 (solid), and O (long dash) as a function of the distance z from the surface.

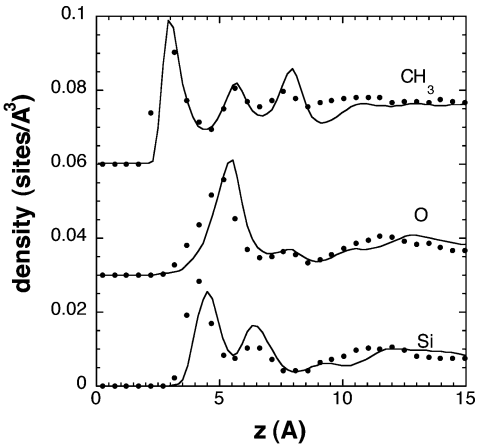

Figure 4. Comparison of density profiles from DFT and full-scale MD simulations of 20-mer PDMS systems. PDMS nonbonded interactions are modeled as repulsive LJ, and the silica−PDMS interaction is modeled using eq 8 (repulsive). The symbols are from MD simulations, and the lines are from DFT calculation. Results of CH_3 and O are shifted upward by 0.06 and 0.03, respectively, for clarity.

for a linear system like polyethylene. Typical medium-induced potentials for the Si, CH_3, and O species are shown in Figure 3. More details on the DFT solution are given later in this Results section.

B. Density Profiles near Surfaces. We present the density profiles obtained from our DFT calculations and MD simulations side by side to provide a direct comparison of the predictions from the two different methods. Note that, however, due to the high requirement of computational resources, we performed MD simulations only on the PDMS80 system.

The first system we studied using density functional theory is a repulsive PDMS80 melt near the repulsive silica surface (eq 8). Figure 4 shows the comparison of the DFT predictions with the MD results for this all-repulsive system. We first attempted to use the PRISM-PY values of the direct correlation functions directly in our DFT solution. However, we found that with the PRISM-PY values of the direct correlation functions the DFT medium-induced potentials were coming out to be too strong, and consequently, it was not possible to reach self-consistency during the DFT solution. We then started to use eq 21 to correct the PRISM-PY results. Following our previous work on polyethylene,[11] we set the multiplicative factor in eq 21 such that the DFT

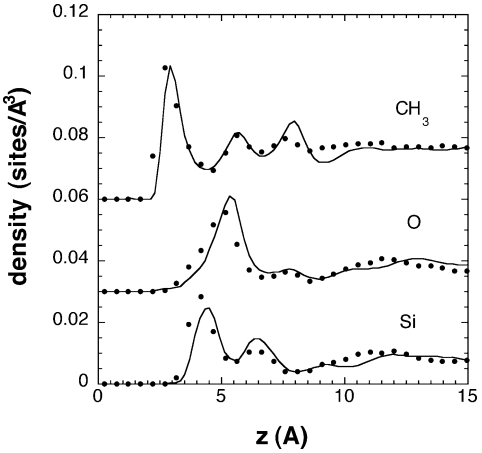

Figure 5. Comparison of density profiles from DFT and full-scale MD simulations of 6-mer PDMS systems. PDMS nonbonded interactions are modeled as repulsive LJ, and the silica−PDMS interaction is modeled using eq 8 (repulsive). The symbols are from MD simulations, and the lines are from DFT calculation. Results of CH_3 and O are shifted upward by 0.06 and 0.03, respectively, for clarity.

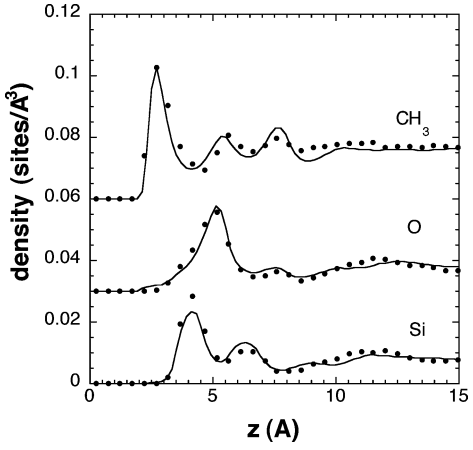

Figure 6. Comparison of density profiles from DFT and full-scale MD simulations of 12-mer PDMS systems. PDMS nonbonded interactions are modeled as repulsive LJ, and the silica−PDMS interaction is modeled using eq 8 (repulsive). The symbols are from MD simulations, and the lines are from DFT calculation. Results of CH_3 and O are shifted upward by 0.06 and 0.03, respectively, for clarity.

calculated density profile predicted the wall contact density with reasonable accuracy. From detailed studies on tangent hard-sphere systems and realistic models of linear polyethylene,[31] it is known that the compressibility predicted from PRISM-PY is always too high (the $c(r)$ values are always too low), and thus one expects that the density profile predicted with PRISM-PY should show less structure (smaller amplitude oscillations) than reality. We observed this expected behavior in our work on polyethylene. Interestingly, here, we observe the opposite trend in our DFT results for repulsive PDMS near a repulsive surface. The medium-induced potentials obtained with the PRISM-PY $c(r)$'s are too strong (which implicitly means that the density profiles would show stronger peaks, if a DFT solution could be obtained) in the case of PDMS. Our calculations on the bulk system shows that, like polyethylene, PRISM predicted compressibility for PDMS is also higher than the corresponding MD value. We found a total structure factor, $H(0)$, value of -0.674 from PRISM compared to a value of -0.97 from MD. The reason for the opposite behavior of the required correction factors in PDMS is thus not obvious and is probably related to the complex balance between the field strength and compressibility. Density profiles predicted from the corrected PRISM-PY direct correlation functions are shown in Figure 4. We used a value of $K_1 = 0.7$ for all six pairs of direct correlation functions.

As seen in Figure 4, DFT predicted density profiles from corrected PRISM-PY correlations are in reasonable agreement with the MD simulation results. In general, the DFT density profiles have more structure compared to their MD counterparts. For CH_3 sites, the location and magnitude of the first peak of the density profile predicted from DFT compare well with those of MD prediction. However, DFT shows more structure away from the surface, which is not seen from MD. For both Si and O sites, the location of the first peak predicted from DFT is slightly out of phase compared to that from MD, but the profiles compare well with MD away from the surface.

Density profiles for the repulsive PDMS near repulsive surfaces for PDMS24 and PDMS48 are shown in Figures 5 and 6. In both cases, we compare our DFT predictions to the MD predictions of the PDMS80 system. Surprisingly, the DFT density profiles for both PDMS24 and PDMS48 compare similarly to that of the PDMS80 system and to the MD density profiles (of the PDMS80 system). The only visible difference between the DFT density profiles of the three systems is that the first peak height of the CH_3 density profile is slightly larger for the smaller PDMS systems. Note here that we have used the same density and temperature in our study of all three systems. In performing the DFT calculations, we have used the same value of K_1 (= 0.7) for all three systems.

As our goal is to study more realistically detailed systems, we turn on the attractions in our systems slowly. First, we performed full many-chain simulations and DFT calculations on systems where the PDMS−silica wall interactions are still modeled with a repulsive interaction (with eq 8), but the PDMS interactions are modeled with the fully attractive LJ interactions. Note that it is possible for such systems to produce dewetting. One should also be careful in dealing with attractive polymer systems, not to be dealing with state conditions where the polymer may exhibit vapor−liquid equilibrium. For our PDMS systems, we chose the system densities on the basis of the experimentally predicted liquid region. Also, from our full-scale MD simulations we did not see any sign of a possible phase separation for this system. As described earlier, we truncate and shift the LJ potential at a distance of 12 Å in modeling the attractive nonbonded interactions in the polymer.

In modeling the long-range interactions for our PRISM-PY predictions through eq 22, we continue to use the same values of K_1 as used for the all-repulsive systems. In our previous work on polyethylene, it was found that the correction factors to the PRISM-PY predicted $c(r)$ values were directly transferable from the all-repulsive system to the attractive systems, and with that, any further corrections to the RPA part of the correlations were not required. Unfortunately, that did not hold true for our study of attractive PDMS near repulsive silica surfaces. In this case, both K_1 and K_2 correction factors were required to obtain reasonable results from the DFT calculation. Once again, we use the procedure of adjusting the density near the wall to obtain a value of K_2.

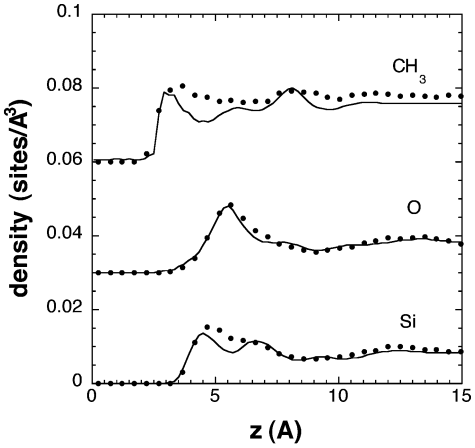

Figure 7. Comparison of density profiles from DFT and full-scale MD simulations of 20-mer PDMS systems. PDMS nonbonded interactions are modeled as full LJ (attractive), and the silica−PDMS interaction is modeled using eq 8 (repulsive). The symbols are from MD simulations, and the lines are from DFT calculation. Results of CH_3 and O are shifted upward by 0.06 and 0.03, respectively, for clarity.

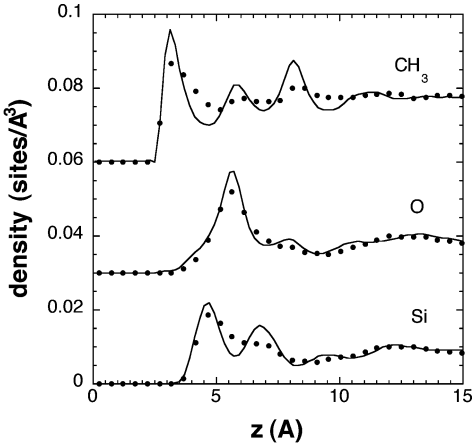

Figure 8. Comparison of density profiles from DFT and full-scale MD simulations of 20-mer PDMS systems. PDMS nonbonded interactions are modeled as full LJ (attractive), and the silica−PDMS interaction is modeled using eq 9 (attractive). The symbols are from MD simulations, and the lines are from DFT calculation. Results of CH_3 and O are shifted upward by 0.06 and 0.03, respectively, for clarity.

By adjusting for the PDMS80 system, we obtain a value of $K_2 = 0.5$. Like K_1, the same K_2 correction factor is applied to all six pairs of correlations. DFT results for density profiles predicted for the attractive PDMS80 system near silica surfaces are displayed in Figure 7, along with the MD results for the same system. As expected, with the attractions added, the polymers pull away from the surface, showing a smaller first peak height in the density profiles. This is observed in both DFT and in the MD results. The general quality of comparison between the DFT and MD density profiles for this system is reasonable and of similar quality to the all-repulsive system. For Si and O site densities, we observe better agreement between DFT and MD generated profiles for the current system in that the location and magnitude of the first peaks are well matched. For the CH_3 site densities, the MD generated profile is very flat compared to the amount of structure observed from the DFT profile.

The next system we look at is the attractive PDMS system near an attractive silica surface (eq 9). In performing DFT calculations for this system, without any further adjustments, we use the same correction factors K_1 and K_2 obtained from the attractive PDMS−repulsive silica surface system. The DFT density profiles for the attractive PDMS80 system near attractive silica surfaces are displayed in Figure 8, along with the corresponding MD results. Once again the DFT profiles compare quite reasonably to the MD profiles. With the attractions between wall and polymer turned on, the first peak height of the density profiles near the surface is increased in both the DFT and MD simulations.

In both the theoretical and simulated profiles in Figures 4−8 it can be seen from the density peak at ∼3 Å that the pendant methyl groups of the PDMS chains are closer to the silica surface than either the oxygen (∼5 Å) or silicon (∼4.5 Å) atoms on the backbone. This might be expected since the methyl groups are more exposed and tend to shield the polymer backbone atoms. Note also that when the forces on atoms near the surface are balanced, as in Figures 4 and 8, there are strong density oscillations resulting from packing effects on the atomic scale. However, when there are strong polymer/polymer attractions with no corresponding polymer/surface attractions as in Figure 7, the polymer tends to dewet from the surface and the density oscillations tend to get washed out. For the case in Figure 8 when both surface and polymer attractive interactions are turned on as expected for PDMS near a silica surface, strong density oscillations are seen in qualitative agreement with experimental surface force measurements.[2,3]

We also performed DFT calculations for the attractive PDMS near both the repulsive and attractive silica surfaces for both PDMS24 and PDMS48 systems and compared those results to the corresponding MD predictions for the PDMS80 system. In all cases, the quality of comparisons was very reasonable irrespective of the chain length of PDMS used in the DFT calculation. This implies that, within the range of chain length studied here for PDMS, the dependence of the density profiles on the chain length is negligible.

Finally, we compare the results of our hybrid/UA PDMS simulations for the fully attractive polymer system next to the 10−4 surface of eq 9 to those from Tsige et al.[4] for a liquid of explicit atom PDMS near an atomistic, amorphous silica surface. Because of the use of different bulk densities in two different studies, we plot the ratio of densities in Figure 9. Despite the differences in the surface polymer interactions used in the two different systems, almost quantitative agreement is observed between the two simulation results. The amplitude of the density peaks and dips compare very well, whereas the overall profiles are slightly out-of-phase from each other. Thus, replacing the atomistic model of the amorphous silica with the integrated LJ surface potential of eq 9 leads to very similar results for the polymer structure near the surface.

C. Stress Profiles and Surface Tension. In this section we compare some physical properties of the silica−PDMS interface as obtained from DFT and MD simulations. We begin with the stress profiles near the surfaces. The only previous detailed investigation of such profiles for polymer thin films was performed by Varnik et al.[43] on a bead−spring polymer melt between repulsive surfaces. As described above, we calculate the components of the pressure tensor directly in the MD simulations. From the DFT, we obtain the stress profile

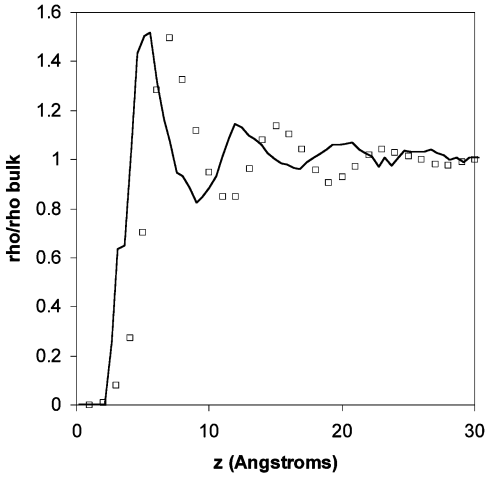

Figure 9. Comparison of density profiles from full-scale MD simulations of hybrid/UA model and explicit atom model. The lines are for the hybrid/UA model (this work), and the symbols are for the explicit atom model (from ref 4).

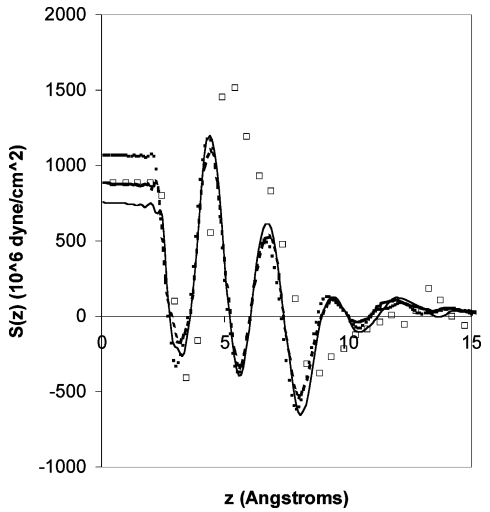

Figure 10. Comparison of stress profiles from DFT and full-scale MD simulations. PDMS nonbonded interactions are modeled as full LJ (attractive), and the silica−PDMS interaction is modeled using eq 8 (repulsive). Meanings of the symbols and lines are as follows: squares (MD simulation of 20-mer PDMS), dotted line (DFT calculation of 6-mer PDMS), dashed line (DFT calculation of 12-mer PDMS), and solid line (DFT calculation of 20-mer PDMS).

in the z-direction $s(z)$ using eq 17 and shift it by a constant to set $s(z) = 0$ in the bulk, as described in the Theory section. Figure 10 shows stress profiles for the attractive PDMS−repulsive silica surface system. Similar to our presentation of the density profiles, we compare DFT predicted stress profiles for all three systems (PDMS24, PDMS48, and PDMS80) with the MD stress profiles for PDMS80. Qualitatively, the profiles from DFT and MD are similar.

Although the physical meaning of the stress profile remains controversial due to the (possible?) nonuniqueness of the transverse component of the stress tensor, the stress profile provides a sensitive comparison between the DFT and MD simulations. Because of the nonuniqueness, it is not a priori clear that the stress profile from density functional theory, obtained from the excess surface free energy, will be the same as the IK stress profile derived from the virial route. However, previous work on mean-field theories found that the same physics applies to the spatial behavior of $P_T(z)$ calculated from the energetic and virial routes.[45] Previous work on lipid bilayers also found a close correspondence between stress profiles from the CMS-DFT and the IK stress in MD simulations on the same molecular model.[27] The same appears to be true here, which is the first comparison of a stress profile for an atomistic polymer in DFT and MD of which we are aware.

The constant region in the stress profiles (Figure 10) near the surface corresponds to the normal pressure in the film. In this region, because of excluded volume, the polymer density is zero, and the only contribution to $s(z)$ is from P_N due to the force of the walls on the fluid. Once the polymer density becomes nonzero, we begin to get other contributions to $s(z)$. The first dip in the stress profile predicted from DFT matches almost exactly with that from MD both in terms of its location and magnitude. The major difference between the DFT and MD predictions is that we have two major peaks in the profile predicted from DFT, whereas we have a very wide peak (covering the two peaks from DFT) in the profile predicted from MD. This difference is somewhat comparable to the differences in the density profiles, in that there was more structure in the DFT predicted profiles.

Like our observations for the density profiles, the stress profiles predicted for the three different lengths of PDMS from our DFT calculations are comparable to each other. The profiles are very much the same throughout the length of the profile, except for the constant region very near the surface corresponding to P_N. We see that at the same temperature and density the normal pressure (bulk pressure) increases with a decrease in chain length. This behavior is consistent with our knowledge of equation of states of small to intermediate sized polymeric molecules. Also, the normal pressure predicted from DFT above is lower than that from MD.

An alternate route to calculating pressure from DFT is using the generated density profiles and the wall sum rule following eq 18. We report the pressures obtained via different routes in Table 2. As one would expect, pressures calculated from DFT using the stress route and the wall sum rule are not completely consistent. However, both routes predict the correct trend in pressure as a function of chain length, and the maximum deviation in calculated pressures between the two routes is about 20%.

We calculate the surface tension from both MD and DFT by directly integrating the stress profiles, following eq 16. We obtain a surface tension value of 47.09 dyn/cm for the PDMS80 system from MD. Our calculated surface tension values from DFT are lower than those

Table 2. Pressure of the PDMS Systems Calculated from Various Routes (in Units of atm)

system	stress route (att wall)	wall sum (att wall)	MD (att wall)	stress route (rep wall)	wall sum (rep wall)	MD (rep wall)
PDMS80	717	813	811	750	762	887
PDMS48	819	1066		882	868	
PDMS24	1021	1196		1070	1259	

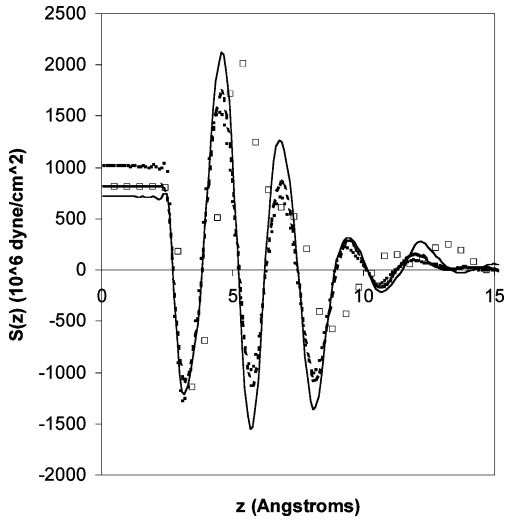

Figure 11. Comparison of stress profiles from DFT and full-scale MD simulations. PDMS nonbonded interactions are modeled as full LJ (attractive), and the silica−PDMS interaction is modeled using eq 9 (attractive). Meanings of the symbols and lines are as follows: squares (MD simulation of 20-mer PDMS), dotted line (DFT calculation of 6-mer PDMS), dashed line (DFT calculation of 12-mer PDMS), and solid line (DFT calculation of 20-mer PDMS).

predicted from MD. From the DFT stress profiles, we obtain surface tension values of 36.09, 36.32, and 28.74 dyn/cm for the PDMS24, PDMS48, and PDMS80 systems, respectively. These values are all of a reasonable magnitude for surface energies.

We also obtain stress profiles for the attractive PDMS−attractive silica surface systems, which are presented in Figure 11. Our comparisons of the stress profiles between DFT and MD predictions and between DFT predictions for various lengths of PDMS are similar to those for the attractive PDMS−repulsive silica surface system. For the attractive surfaces, we obtain a MD surface tension value of 46.32 dyn/cm for PDMS80. DFT surface tension values for this system are 24.27, 21.5, and 22.45 dyn/cm for the PDMS24, PDMS48, and PDMS80 systems, respectively. Surprisingly, DFT predicted surface tensions match quite well with the experimentally determined surface tension value of 22 dyn/cm for PDMS near silica surface.[46]

Normal pressures from DFT calculated via the stress route and the wall-sum route for the attractive PDMS−attractive silica surface systems are also reported in Table 2. In principle, the normal pressure of the system should only depend on the polymer and should be completely independent of the surface interactions. Our results are reasonably consistent with this requirement.

VI. Conclusions

Properties for realistically detailed PDMS melts confined between silica surfaces have been calculated using the structure based density functional theory of Chandler, McCoy, and Singer and compared to molecular dynamics simulations. The primary input to the density functional theory, the direct correlation function, was obtained using the self-consistent PRISM theory with the PY closure for the repulsive potentials and then correcting for the attractive LJ tail via use of the random-phase approximation.

For purely repulsive systems and linear molecules, it is known that a cancellation of errors occurs between the large compressibility from PRISM and the field predicted from eq 11 (which is known to be too strong). For polyethylene this cancellation was found to be inadequate in a previous study,[11] and empirical corrections to the direct correlation functions using a multiplication factor greater than 1.0 were required to obtain reasonable agreement between density profiles predicted from DFT and full-scale simulations. For PDMS, in this work, we observed an opposite trend in that PRISM-PY predicted the direct correlation functions are too strong and a multiplication factor smaller than 1.0 is required to correct the direct correlation functions to obtain reasonable agreement between DFT and full-scale simulations. When the appropriate empirical corrections are applied to the direct correlation functions, the DFT predicted density profiles compare reasonably with those of MD simulation.

To include the effect of polymer attractions on the density profile, we also made multiplicative corrections to the PRISM-PY generated direct correlation function while adding the RPA tail correction. In the study on polyethylene near surfaces,[11] it was found that even for attractive systems, either only a correction to the PRISM-PY generated direct correlation function for the core system or a correction to the RPA tail was sufficient to obtain good agreement between density profiles from DFT and simulations. Unfortunately, that did not hold true for our study of attractive PDMS systems. Here, two separate multiplicative correction factors were required simultaneously on both the PRISM-PY predicted part and the RPA part of the direct correlation function.

We also studied the stress profiles and surface tension using both the DFT and MD simulations. Like the density profiles, DFT predicted stress profiles also compare reasonably with those predicted from MD simulations. In general, DFT predicted stress profiles show more structure compared to their MD counterparts. Surface tensions predicted from DFT were lower than those predicted from MD simulations.

We studied properties of PDMS of three different chain lengths, namely 6-mer, 12-mer, and 20-mer, using DFT. Within the range of chain lengths studied here, the generated density profiles and stress profiles appeared to be very similar and did not depend significantly on the chain sizes. However, it is possible that with a significantly different chain size the predicted profiles would be different then those predicted for our medium-sized PDMS chains.

We have demonstrated in this study that a DFT theory is capable of describing atomistic models of complex polymers near surfaces with moderate accuracy. This is the first study of this kind where an atomistically detailed model of a complex polymer as PDMS has been studied using DFT theory with good success. This opens the possibility to study many important problems related to complex polymers near surfaces at the atomistic level. Such problems include polymer mixtures near surfaces, polymer adhesion, polymers in confined geometries, and polymer nanocomposites.

Acknowledgment. We thank Mark Stevens for helpful discussions and assistance with the code for calculating the stress tensor and Frank van Swol, Jeff Hoyt, and Laura Frink for helpful discussions about stress profiles in inhomogeneous fluids. Sandia is a multiprogram laboratory operated by Sandia Corpora-

tion, a Lockheed Martin Company, for the United States Depart of Energy's National Nuclear Security Administration under Contract DE-AC04-94AL85000.

References and Notes

(1) Rutnakornpituk, M.; Baranauskas, V. V.; Riffle, J. S.; Connolly, J.; St. Pierre, T. G.; Dailey, J. P. *Eur. Cells Mater*. **2002**, *3*, 102.
(2) Horn, R. G.; Israelachvili, J. N. *Macromolecules* **1988**, *21*, 2836.
(3) Israelachvili, J. N.; Adams, G. E. *J. Chem. Soc., Faraday Trans. 1* **1978**, *74*, 975.
(4) Tsige, M.; Soddemann, T.; Rempe, S. B.; Grest, G. S.; Kress, J. D.; Robbins, M. O.; Sides, S. W.; Stevens, M. J.; Webb III, E. *J. Chem. Phys.* **2003**, *118*, 5132.
(5) Chandler, D.; McCoy, J. D.; Singer, S. J. *J. Chem. Phys.* **1986**, *85*, 5971.
(6) Chandler, D.; McCoy, J. D.; Singer, S. J. *J. Chem. Phys.* **1986**, *85*, 5977.
(7) McCoy, J. D.; Singer, S. J.; Chandler, D. *J. Chem. Phys.* **1987**, *87*, 4853.
(8) Sen, S.; Cohen, J. M.; McCoy, J. D.; Curro, J. G. *J. Chem. Phys.* **1994**, *101*, 3205.
(9) Sen, S.; McCoy, J. D.; Nath, S. K.; Donley, J. P.; Curro, J. G. *J. Chem. Phys.* **1994**, *102*, 3431.
(10) Flory, P. J. *Statistical Mechanics of Chain Molecules;* Wiley: New York, 1969.
(11) Nath, S. K.; Curro, J. G.; McCoy, J. D. *J. Phys. Chem. B* **2005**, *109*, 6620.
(12) For a review see: Schweizer, K. S.; Curro, J. G. *Adv. Chem. Phys.* **1997**, *98*, 1. Schweizer, K. S.; Curro, J. G. *Adv. Polym. Sci.* **1994**, *116*, 321.
(13) Hansen, J. P.; McDonald, I. R. *Theory of Simple Liquids*, 2nd ed.; Academic: London, 1986.
(14) Woodward, C. E.; Yethiraj, A. *J. Chem. Phys.* **1994**, *100*, 3181. Yethiraj, A.; Woodward, C. E. *J. Chem. Phys*. **1995**, *102*, 5499.
(15) Patra, C. N.; Yethiraj, A. *J. Chem. Phys.* **2003**, *118*, 4702. Muller, M.; MacDowell, L. G.; Yethiraj, A. *J. Chem. Phys*. **2003**, *118*, 2929.
(16) Forsman, J.; Woodward, C. E.; Freasier, B. C. *J. Chem. Phys.* **2002**, *116*, 4715.
(17) Christopher, P. S.; Oxtoby, D. W. *J. Chem. Phys.* **2003**, *119*, 10330.
(18) Hooper, J. B.; McCoy, J. D.; Curro, J. G. *J. Chem. Phys.* **2000**, *112*, 3090.
(19) Frischknecht, A. L.; Curro, J. G. *Macromolecules* **2003**, *36*, 2122.
(20) Heine, D. R.; Grest, G. S.; Lorenz, C. D.; Tsige, M.; Stevens, M. J. *Macromolecules* **2004**, *37*, 3857.
(21) The original force field as published in ref 19 contained two errors. First, the units for the angle bending energy in Table 1 of ref 19 should be kcal/(mol rad^2), not kcal/(mol deg^2) as written. Second, a calculation error leads to slightly incorrect values of the LJ diameters σ for the Si$-$CH$_3$ and O$-$CH$_3$ interactions. When calculated as described in ref 31, these values should have been $\sigma = 3.72$ Å for Si$-$CH$_3$ and $\sigma = 3.29$ Å for O$-$CH$_3$, rather than the values given in Table 2 of ref 19. However, a simulation of bulk PDMS with the corrected values led to essentially no changes the intermolecular correlation functions $g_{\alpha\beta}(r)$. In this work, we used the originally published values as shown in Table 2.
(22) For a review see: McCoy, J. D.; Nath, S. K. *Chemical Applications of Density Functional Theory*; Laird, B. B., Ross, R. B., Ziegler, T., Eds.; American Chemical Society: Washington, DC, 1996.
(23) Allen, M. P.; Tildesley, D. J. *Computer Simulation of Liquids*; Clarendon Press: Oxford, 1987.
(24) Henderson, J. R.; van Swol, F. *Mol. Phys.* **1984**, *51*, 991.
(25) Henderson, J. R. Statistical Mechanical Sum Rules. In Henderson, D., Ed.; *Fundamentals of Inhomogeneous Fluids*; Dekker: New York, 1992.
(26) Rowlinson, J. S.; Widom, B. *Molecular Theory of Capillarity*; Clarendon Press: Oxford, 1982.
(27) Frink, L. J. D.; Frischknecht, A. L. *Phys. Rev. E*, in press. Frischknecht, A. L.; Frink, L. J. D. *Phys. Rev. E*, in press.
(28) Rickayzen, G. *Mol. Phys.* **1985**, *55*, 161.
(29) Chandler, D.; Andersen, H. C. *J. Chem. Phys.* **1972**, *57*, 1930. Chandler, D. In *Studies in Statistical Mechanics VIII*; Montroll, E. W., Lebowitz, J. L., Eds.; North-Holland: Amsterdam, 1982; p 274.
(30) Livadaru, L.; Kovelenko, A. *J. Chem. Phys.* **2004**, *121*, 4449.
(31) Curro, J. G.; Webb III, E. B.; Grest, G. S.; Weinhold, J. F.; Putz, M.; McCoy, J. D. *J. Chem. Phys.* **1999**, *111*, 9073.
(32) Sides, S. W.; Curro, J. G.; Grest, G. S.; Stevens, M. J.; Soddemann, T.; Habenschuss, A.; Londono, J. D. *Macromolecules* **2002**, *35*, 6455.
(33) Sok, R. M.; Berendsen, H. J. C. *J. Chem. Phys.* **1992**, *96*, 4699.
(34) Frischknecht, A. L.; Curro, J. G. *J. Chem. Phys.* **2004**, *121*, 2788.
(35) van Swol, F.; Henderson, J. R. *Phys. Rev. A* **1991**, 2932.
(36) Plimpton, S. J. *J. Comput. Phys.* **1995**, *117*, 1.
(37) Irving, J. H.; Kirkwood, J. G. *J. Chem. Phys.* **1950**, *18*, 817.
(38) Schofield, P.; Henderson, J. R. *Proc. R. Soc. London A* **1982**, *379*, 231.
(39) Wajnryb, E.; Altenberger, A. R.; Dahler, J. S. *J. Chem. Phys.* **1995**, *103*, 9782.
(40) Harasima, A. *Adv. Chem. Phys.* **1958**, *1*, 203.
(41) Hafskjold, B.; Ikeshoji, T. *Phys. Rev. E* **2002**, *66*, 011203.
(42) Goetz, R.; Lipowsky, R. *J. Chem. Phys.* **1998**, *108*, 7397.
(43) Varnik, F.; Baschnagel, J.; Binder, K. *J. Chem. Phys.* **2000**, *113*, 4444.
(44) Hardy, R. J. *J. Chem. Phys.* **1982**, *76*, 622.
(45) Oversteegen, S. M.; Barneveld, P. A.; Leermakers, F. A. M.; Lyklema, J. *Langmuir* **1999**, *15*, 8609.
(46) Emerson, J., private communications.

MA051001K